Contents lists available at ScienceDirect

Solar Energy Materials and Solar Cells

Comparison of different types of interfacial oxides on hole-selective p+-poly-Si passivated contacts for high-efficiency c-Si solar cells

Xueqi Guo [a,1], Mingdun Liao [a,1], Zhe Rui [a], Qing Yang [a,b], Zhixue Wang [a], Chunhui Shou [c], Waner Ding [c], Xijia Luo [d], Yuhong Cao [d], Jiaping Xu [d], Liming Fu [d], Yuheng Zeng [a,**], Baojie Yan [a,*], Jichun Ye [a,***]

[a] Ningbo Institute of Material Technology and Engineering, Chinese Academy of Sciences, Ningbo City, Zhejiang Province, 315201, PR China
[b] University of Chinese Academy of Sciences, Beijing, 100049, PR China
[c] Zhejiang Energy Group R&D, Hangzhou, Zhejiang Province, 310003, PR China
[d] Scenergy Technology Co., Ltd, Changzhou City, Jiangsu Province, PR China

ARTICLE INFO

ABSTRACT

We present a systematic study of highly boron (B)-doped poly-silicon (p+-poly-Si) and ultrathin silicon oxide (SiO$_x$) bi-layer structure, also named as p-TOPCon, as the hole-selective passivated contact on n-type c-Si wafer, where the SiO$_x$ layer is made with three methods of hot nitric acid oxidation SiO$_x$ (NAOS-SiO$_x$), plasma-assisted nitrous-oxide (N$_2$O) gas oxidation (PANO-SiO$_x$), and thermal oxidation (Thermal-SiO$_x$). We demonstrate that the SiO$_x$ has a strong influence on the passivation quality. The best result is achieved using the Thermal-SiO$_x$, while the NAOS-SiO$_x$ is slightly inferior, but better than the PANO-SiO$_x$. The p+-poly-Si/SiO$_x$ structures with the three SiO$_x$ layers achieve the optimized passivation quality at different annealing temperatures of 820 °C for the NAOS-SiO$_x$, 880 °C for the PANO-SiO$_x$, and 930 °C for the Thermal-SiO$_x$. The other potential factors affecting the passivation quality are also studied. The most important observation is that the optimized p-TOPCon structures with the three SiO$_x$ layers have a similar B diffusion profile, which penetrates into the c-Si wafer about 50 nm with B concentration decreasing to $\sim 1 \times 10^{18}$ cm^{-3}. However, the overall p+-poly-Si/SiO$_x$ is still much poorer than n+-poly-Si/SiO$_x$ in terms the passivation quality. The comparison of the τ_{eff} versus carrier injection intensity spectra suggests that the B–O complex is the passivation killer possibly, and the approaches to improve the p-TOPCon are searching the other elements to reduce the B–O defects. In addition, contact resistivity (ρ_c) measurements show that the Thermal-SiO$_x$ leads a higher ρ_c than the others, but its value is still low enough for high-efficiency solar cells.

1. Introduction

Carrier selective passivated contact using ultrathin silicon oxide (SiO$_x$) and highly doped poly-silicon (poly-Si) becomes an advanced high-efficiency crystalline silicon (c-Si) solar cell technology heading to the mass production of high-efficiency solar panels [1–6]. Although this concept has been proposed to improve c-Si solar cell performance, especially open-circuit voltage, for a long time [7,8], it has only got serious attention since the remarkable efficiency improvements achieved by the Fraunhofer ISE with the record cell efficiency of 25.7% [1,

2]. They named the cell structure as TOPCon, from the abbreviations of tunnel oxide passivated contact with the assumption of carrier transporting through the SiO$_x$ layer by quantum tunneling, although the transport through pinholes has been found to be dominant in some cases [9,10]. By reflecting the uncertainty in the carrier transport mechanisms and different cell structures, and probably from the commercialization point of consideration, other names such as POLO [3], PERPoly [4], monoPoly [5], and i-TOPCon [6] are also used.

From the survey on the literature, one may see that most of the works are carried out using highly phosphorus (P)-doped n+-poly-Si/SiO$_x$,

---

* Corresponding author.
** Corresponding author.
*** Corresponding author.
E-mail addresses: yuhengzeng@nimte.ac.cn (Y. Zeng), yanbaojie@nimte.ac.cn (B. Yan), jichun.ye@nimte.ac.cn (J. Ye).
[1] equal contribution as the first author.

named as n-TOPCon, on n-type c-Si wafers [1–6], because of the excellent passivation quality and high solar cell efficiency. While a limited number of the counterpart of highly boron (B)-doped p^+-poly-Si/SiO$_x$ (p-TOPCon) has been studied and shown the poorer passivation quality than the n-TOPCon irrespective of the doping type of the wafers [11–22]. However, the p-TOPCon on p-type c-Si wafer would have a high impact on the solar photovoltaic (PV) industry if it could also have a great passivation quality because it might be directly used in upgrading the passivated emitter and rear cell (PERC) production line, which uses the same front P-diffused emitter and only changes the backside procedures with a limited modifications. In addition, the p-TOPCon is also used in double-side TOPCon solar cells on n-type c-Si wafer by replacing the B-diffused emitter with the p-TOPCon [11,23] or rear emitter n^+-n-p^+ structured double-side TOPCon solar cells for high-efficiency perovskite/c-Si double-junction solar cells. In addition, the p-TOPCon could be used locally underneath the front metal contact of conventional n-TOPCon solar cells as the selective emitter. Therefore, improving the passivation quality of p-TOPCon has a great significance for the solar photovoltaic industry.

The p-TOPCon was studied as early as the n-TOPCon, but showing a poorer passivation quality [12] with an implied open-circuit voltage (iV_{oc}) of 680 mV than the achieved 725 mV using the n-TOPCon. Mack et al. [13] improved the p^+-poly-silicon passivation quality and found a strong effect of wafer surface morphology on the p-TOPCon passivation quality and the surface with the saw damage etched wafer exhibiting better surface passivation than textured wafers. They achieved a high iV_{oc} of 737 mV and fabricated large area (244 cm^2) p-TOPCon solar cell on p-type c-Si wafer with an efficiency of 20.4% [14]. The EPFL group made the p^+-poly-Si on p-type c-Si made using TMB as the B-doping gas and investigated the annealing temperature and time as well as the hydrogenation effect on the passivation quality. They achieved an iV_{oc} of 718 mV and an efficiency of 21.9% [15,16]. The ECR/TNO group implemented a novel dielectric stacked-layer structure as the source of hydrogenation, modified the B-diffusion profile, and then achieved a passivation level of single-sided saturated current density ($J_{0,S}$) of ~3 fA/cm^2 and iV_{oc} of 735 mV with p^+-poly-Si on n-type wafer [17]. Yan et al. used a co-sputtering method to make p^+-poly-Si as the hole selective passivated contact on p-type c-Si wafers and achieved an efficiency of 23% [18]. For improving the adhesion and making blister-free poly-Si on the SiO$_x$ coated c-Si wafer, Morisset et al. used high hydrogen dilution (R = 50) to reduce the possibility of blistering formation and improved the passivation quality. They used p^+-poly-Si on n-type c-Si and achieved an iV_{oc} of 714 mV [19]. The SERIS group used Al$_2$O$_3$ to substitute SiO$_x$ and achieved the excellent iV_{oc} of 723 mV and $J_{0,S}$ of 6.6 fA/cm^2 [20]. The NREL group has also studied both the n-TOPCon and p-TOPCon structures systematically to improve the passivation quality [21] by the defect passivation using various hydrogen treatments [22] and the optimization of the SiO$_x$ thickness [23]; they achieved an iV_{oc} of over 710 mV with p-TOPCon on n-type c-Si wafers and identified the hydrogenation effect by substituting hydrogen with deuterium [22]. Furthermore, they replaced B by Ga to reduce the B–O complex defects, improved the passivation quality, and reached i$V_{oc} \geq$730 mV [24]. The Fraunhofer ISE group studied the SiO$_x$ layers grown with different methods and their effects on the passivation quality, and found that the thermally grown SiO$_x$ has a high tolerance for high-temperature annealing [25–27]; they recently did a comparison study of n-TOPCon and p-TOPCon on n-type c-Si wafers and achieved an iV_{oc} of 730 mV and 705 mV, respectively. They found that the B-diffusion can be suppressed by using a silicon-nitride-oxide made with plasma oxidation, but the damage on the SiO$_x$ by the incorporation of nitrogen still caused a poorer passivation quality with the p^+-poly-Si [27]. Similarly, the ISFH group did comparison studies of p^+-poly-Si/SiO$_x$ and n^+-poly-Si/SiO$_x$ on n-type and p-type c-Si wafers. They found that in general the p^+-poly-Si/SiO$_x$ produces poorer passivation quality than n^+-poly-Si/SiO$_x$, and the p-type c-Si wafers are more difficulty to be passivated than the n-type wafers and proposed the B–O pairs are responsible for the poorer passivation [28–30].

It is clear that the p^+-poly-Si/SiO$_x$ does not provide a high passivation quality as the n^+-poly-Si/SiO$_x$ does. Especially, the solar cell efficiency achieved using p-TOPCon [18] is still much lower than using n-TOPCon [2] and even lower than the record efficiency of p-type PERC solar cell. Ideally, the p-TOPCon solar cell should have a higher efficiency than p-type PERC solar cell; however, such expectation has not been reached yet. Two reasons could be behind: first, the amount of optimizations on the p-TOPCon solar cell is not enough; and second, fundamentally, p-TOPCon has its limitation, such as the recombination through B–O complex defects. The p-TOPCon indeed removes the metal/c-Si contact recombination in the p-type PERC solar cells, but the B-doped poly-Si/SiOx might induce additional B–O complex defects. Therefore, the investigation of B-doped p-TOPCon has a significance for solar industry no matter on n-type or p-type c-Si wafers. The fundamental question is what is the root cause for the poorer passivation with B-doped p^+-poly-Si/SiO$_x$ than P-doped n^+-poly-Si/SiO$_x$; the technique question is what (if any) are the approaches for improving B-doped p^+-poly-Si/SiO$_x$ passivation quality and the p-TOPCon solar cell efficiency. The root cause could be in the p^+-poly-Si, SiO$_x$, SiO$_x$/c-Si interface, and the B-diffusion layer penetrated into the c-Si. Unless the origins of the deterioration are figured out, the route for achieving a high quality passivation with B-doped p^+-poly-Si/SiO$_x$ is difficult to be paved. Therefore, the objectives of this work are to compare the passivation quality of p^+-poly-Si/SiO$_x$ with the ultrathin SiO$_x$ layers made with different methods and to check whether the SiO$_x$ properties have any significant impacts on the passivation quality, and furthermore to search for an optimized fabrication procedure to make high-quality B-doped p-TOPCon structure for high-efficiency solar cells. We made the ultrathin SiO$_x$ layers with three methods of hot nitric acid oxidation (NAOS-SiO$_x$), plasma-assisted nitrous-oxide (N$_2$O) gas oxidation (PANO-SiO$_x$), and thermal oxidation (Thermal-SiO$_x$), and demonstrated that the SiO$_x$ has a strong influence on the passivation quality. The best result is achieved using the Thermal-SiO$_x$. The NAOS-SiO$_x$ is slightly inferior, but better than the PANO-SiO$_x$. The p-TOPCon structures with the three SiO$_x$ layers achieve the optimized passivation quality at different annealing temperatures, and the optimized p-TOPCon structures with the three SiO$_x$ layers have a similar B diffusion profile. Comparing with the n^+-poly-Si/SiO$_x$, it reveals that the overall p^+-poly-Si/SiO$_x$ has a poor the passivation quality with a significantly degraded the effective minority carrier lifetime (τ_{eff}) at the low injection levels, indicating the Shockley-Read-Hall (SRH) recombination through deep-level defects [31,32]. Therefore, we believe that the technique approach to improve the p^+-poly-Si/SiO$_x$ passivation quality is to reduce the deep level interface defects that might be related to the B–O complex.

2. Experimental details

The samples for the passivation study were made on solar-grade ~3 Ω cm 170-μm n-type CZ c-Si wafers. In each run, four 4 × 4 cm^2 square substrates cut from 156 × 156 cm^2 wafers were used for checking the experimental uniformity and reproducibility. After a standard RCA cleaning, each wafer was immersed in the 5% HF solution to remove the native oxide layer formed during the cleaning process. And then, an ultrathin SiO$_x$ layer grown on both sides in (i) a hot HNO$_3$ bath at 110 °C for 15 min (NAOS-SiO$_x$), (ii) an N$_2$O plasma for 5 min in a plasma-enhanced chemical vapor deposition (PECVD) system (13.56 MHZ) (PANO-SiO$_x$), and (iii) a tube furnace at 650 °C for 20 min within an N$_2$ and O$_2$ atmosphere (Thermal-SiO$_x$). On top of the thin SiO$_x$ layer, a 40-nm thick B-doped hydrogenated amorphous silicon (p^+-a-Si:H) was deposited on the single side for contact resistivity measurements or both-side for the passivation quality measurements in the same PECVD system as the PANO-SiO$_x$ fabrication. As a reference, a 40-nm thick P-doped a-Si:H (n^+-a-Si:H) was also made to form n-TOPCon structures. The samples with the three different ultrathin SiO$_x$ layers were annealed in a diffusion annealing furnace at different temperatures ranging
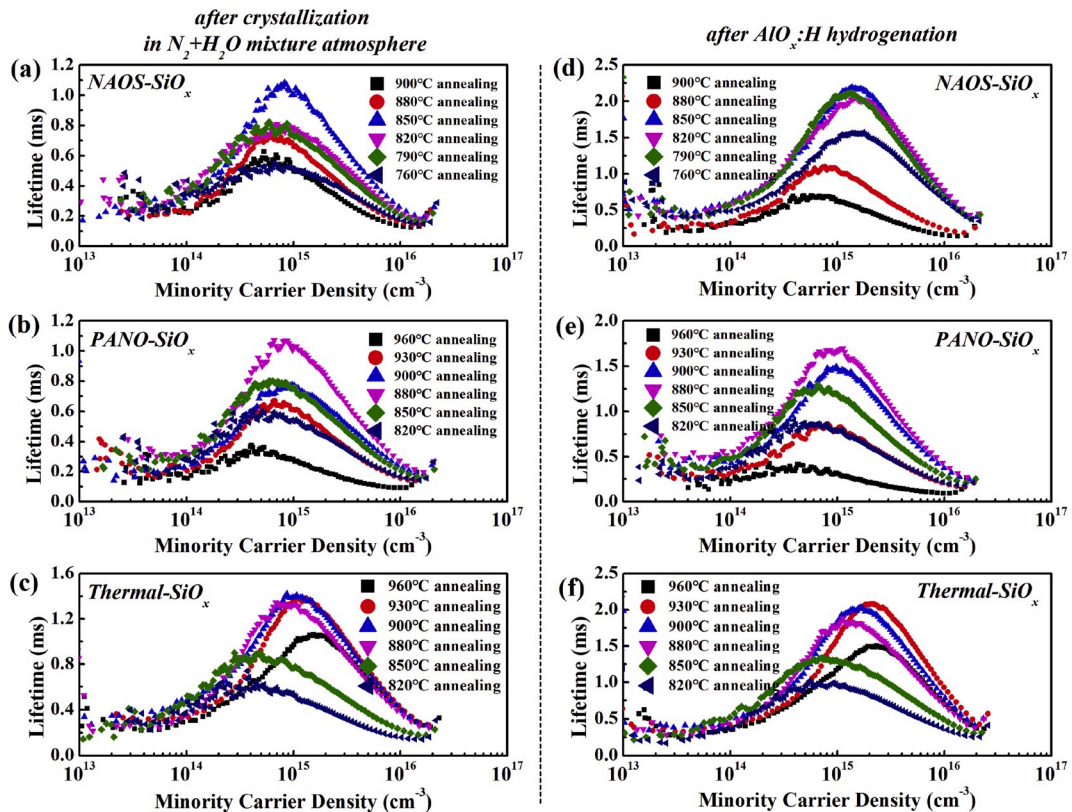
between 760 °C and 960 °C for 30 min in a high-purity N_2 atmosphere with a hydrogenation process incorporated with bringing in water vapor carried by N_2 at 450 °C during the cooling process [33]. For the double-side passivated samples, a thin AlO_x:H was deposited by atomic-layer-deposition (ALD) for the further improvement of surface passivation.

A Sinton lifetime tester (WCT-120) was used to measure conductance decay, from which the τ_{eff}, iV_{oc}, and $J_{0,S}$ were extracted for passivation quality characterization. The crystalline structure of the p^+-poly-Si layer was measured using Raman spectroscopy with a 325 nm excitation laser to avoid the influence of the c-Si wafer substrate [34]. An electrochemical capacitance-voltage (ECV) measurement system (Buchanan, CVP21) was used to measure the dopant concentration profiles of the annealed samples. For contact resistivity measurements, dark current versus voltage (I–V) characteristics was measured on the single-side p-TOPCon coated samples, where Al contacts with various gap distances were thermally evaporated through shadow masks on the p-TOPCon coated side to form an Ohmic contact between the metal and the poly-Si layers. The native SiO_x was removed by dipping the sample in diluted HF before loading the sample into the chamber to ensure the contact resistance is not affected by the native SiO_x. The contact resistivity between the metal and the p^+-poly-Si was calculated with the transmission line method (TLM) [35] from the I–V data measured across different gap widths between two Al electrodes, by which the contribution from the poly-Si layer is removed, and the accurate contact resistivity can be obtained. For solar cell application, the contact resistance across the SiO_x layer is also a critical parameter, but the current flow in the TLM measurement is mainly in the p^+-ploy-Si layer, which misses the contact resistance across the SiOx. Furthermore, the diode characteristic formed by the p^+-poly-Si and n-c-Si wafer prevents the accuracy of contact resistance analysis using the Cox-Strack (CS) method [36] although an improved analysis has been proposed to take care the non-Ohmic contact [37,38]. Here, we made n-TOPCon structures with the three SiO_x layers on the n-type c-Si wafer and measured I–V characteristics of single-side passivated samples, on which circular Al electrodes with different diameters were deposited on the top surface, and a whole area electrode was formed by GaSn paste on the back, which forms an Ohmic contact with n-type c-Si. The contact resistivity values were extracted from the linear I–V characteristics measured on the circular electrodes with different areas using the CS method, by which the contributions from the current spreading outside the electrodes are calibrated out. The interfacial chemical bonding configurations of the SiO_x were characterized using an X-ray photoelectron spectroscopy (XPS) (AXIS ULTRA DLD).

3. Results and discussion

Hot nitric acid oxidation has been widely used for making ultrathin SiO_x [39]. In addition to the NAOS-SiO_x, we have preciously optimized the SiO_x fabrication processes using mixed acids at low temperature and using N_2O PECVD oxidation [40–42]. We used the optimized process for making the SiO_x layers in this study, where the thicknesses of the SiO_x layers are 1.8 ± 0.2 nm, 1.5 ± 0.2 nm, and 1.8 ± 0.2 nm for the NAOS-SiO_x, PANO-SiO_x, and Thermal-SiO_x, respectively, as measured with TEM and shown later. Here, the same 40-nm thick a-Si:H layer but doped with B were used as the p^+-poly-Si precursor on the symmetrically double-side passivated samples. We did systematic annealing studies by monitoring the τ_{eff} versus injection intensity as a function of annealing temperature with the results shown in Fig. 1, where the spectra in the left panel were recorded after the crystallization annealing with hydrogenation by moisture/nitrogen annealing starting at 450 °C during the cooling process [33] and the right ones after the additional hydrogenation with the ALD grown AlO_x:H capping and annealing. The observations are made below. First, all of the spectra show a

Fig. 1. The τ_{eff} versus injection intensity spectra of three sets of double-side passivated n-type c-Si with p^+-poly-Si/SiO_x, where the SiO_x layers were made with different methods. The left panels are in the hydrogenated state with the moisture/nitrogen annealing and the right after additional hydrogenation with AlO_x:H capping and annealing.

mountain-like shape with a peak in the middle of the plot, decrease with the increase of the injection level in the high injection side, and decrease as well with the decrease of the injection level in the low injection side, which is very different from the n$^+$-poly-Si passivated contact with a monotonic decrease with the increase of injection level as shown in Fig. 2 (a). Second, the overall lifetime increases with the increase of annealing temperature and reach an optimized condition and then decreases with the increase of annealing temperature further. Third, the peak of τ_{eff} shifts to the high injection level with the improvement of the passivation quality. Through comparing the spectra in Fig. 2, not only the absolute τ_{eff} (a) and the implied open-circuit voltage (b) under the illumination are much higher with the n-TOPCon than with the p-TOPCon, but also the shape of τ_{eff} (a) versus injection intensity spectra are very different, indicating additional recombination occurs in the p-TOPCon passivated samples. The mountain-like shape spectra is the signature of recombination through deep-level defects, which might be attributed to B–O complex recombination [43–45] as observed only in the p$^+$-poly Si or on p-type Si wafers. The same assignment has been made by Winter et al. [30]. Therefore, we believe that the technique approach to improve the p-TOPCon passivation quality is to reduce the B–O complex defect density with either different dopants such as gallium (Ga) [24] or aluminum (Al), or using O free dielectric passivation layers such as ultrathin SiN$_x$ or something else.

For a clear comparison on the passivation quality with different SiO$_x$ layers, we extracted three characteristic passivation parameters of the τ_{eff} at the injection level of 1×10^{15} cm^{-3}, iV_{oc}, and $J_{0,S}$. Fig. 3 plots the passivation parameters as a function of annealing temperature, where the same as in Fig. 1, the left plots are the state after crystallization and moisture/nitrogen hydrogenation, and the right ones with additional hydrogenation by ALD AlO$_x$:H capping and annealing. The results show that 1) the additional hydrogenation by the ALD AlO$_x$:H capping and annealing adds a noticeable improvement as previously observed [33], 2) each set of the data has an optimized annealing temperatures at 820 °C, 880 °C, and 930 °C for the NAOS-SiO$_x$, PANO-SiO$_x$, and Thermal-SiO$_x$, respectively, and 3) the best passivation with iV_{oc} = 722 mV, τ_{eff} = 1.56 ms at 1×10^{15} cm^{-3}, and $J_{0,S}$ = 5.95 fA/cm^2 is achieved using the Thermal-SiO$_x$ annealed at 930 °C, the mediocre with iV_{oc} = 718 mV, τ_{eff} = 1.85 ms at 1×10^{15} cm^{-3}, and $J_{0,S}$ = 7.9 fA/cm^2 using the NAOS-SiO$_x$, and the worst with iV_{oc} = 703 mV, τ_{eff} = 1.65 ms at 1×10^{15} cm^{-3}, and $J_{0,S}$ = 18.5 fA/cm^2 using the PANO-SiO$_x$. It is noted that the iV_{oc} of Thermal-SiO$_x$ sample is higher than the one with NAOS-SiO$_x$ or PANO-SiO$_x$, which may result from the improved chemical passivation of interfacial SiO$_x$ with a closing stoichiometry configuration as shown later on and the enhanced impurity gettering by the rising annealing temperature [46].

From the above results, one can see that the SiO$_x$ layer has a strong influence on the passivation quality. Each category of the SiO$_x$

corresponds to an optimized annealing temperature. Let us consider the possibilities, the high-temperature annealing and hydrogenation result in the following structural, compositional, and electronic changes, including 1) the a-Si:H film crystallization to poly-Si, 2) the dopant activation, diffusion through the SiO$_x$, and penetration into the c-Si wafer, and 3) dangling termination by hydrogen atoms. Next, we explore the origin of causing the different passivation behaviors by checking each of the potential dominant factors. First, we checked whether the poly-Si layers on the different SiO$_x$ layers have different crystalline structures by the UV-Raman spectroscopy with the results shown in Fig. 4, where the normalized data of the Raman spectra were taken from the p$^+$-poly-Si layers on the three kinds of SiO$_x$ annealed at the same annealing temperature (880 °C). The measurements were made with a UV (325 nm) excitation to avoiding the contribution from the c-Si substrates [34]. From the results, it appears that the three samples have very similar Raman spectra and similar crystallization ratio on the same annealing temperature, indicating that the crystalline structure of the p$^+$-poly-Si is not affected by the underneath SiO$_x$ layer and therefore the crystalline structure is not a key factor determining the passivation quality in this case.

The second change is the dopant activation and diffusion. It is well known that the doping efficiency in a-Si:H is very low because of the balance between the dopant associated defect generations with the three-coordinated configuration and the four-coordinated doping coordination as well as the carrier trapping in the band tails [47,48]. The high-temperature annealing crystalizes the a-Si:H into poly-Si, and at the same time, the band tail narrows down or disappears, and therefore the doping efficiency is increased significantly. In addition, the high density of dopants in the poly-Si leads to a forward diffusion through the SiO$_x$ and penetration into the c-Si wafer. To check the dopant activation and diffusion, we measured the dopant distribution profiles in the samples annealed at different temperatures. Fig. 5 shows a few examples of the measurement results, where (a), (b), and (c) are the active B distributions of the samples with the NAOS-SiO$_x$, PANO-SiO$_x$, and Thermal-SiO$_x$, respectively, and (d) compares the samples annealed at the optimized temperatures with the three kinds of SiO$_x$ layers. Generally speaking, the B distribution curves have the similar shape with a flat part in the p$^+$-poly-Si, a narrow curb appears in the SiO$_x$ region, and a long tail is extending into the c-Si wafer. Looking at the p$^+$-poly-Si layer, the active B concentrations are reasonably high in the range around 1–2 $\times 10^{20}$ cm^{-3}, indicating a high activation rate achieved after the high-temperature annealing; comparing the distribution profiles of a given sample annealed at different temperatures, the diffusion tail in the c-Si wafer widens significantly with the increase of the annealing temperature; the three samples with different SiO$_x$ at their optimized temperatures have a similar B diffusion profile, which penetrates into the c-Si wafer about 50 nm with B concentration decreasing to ~1×10^{18}
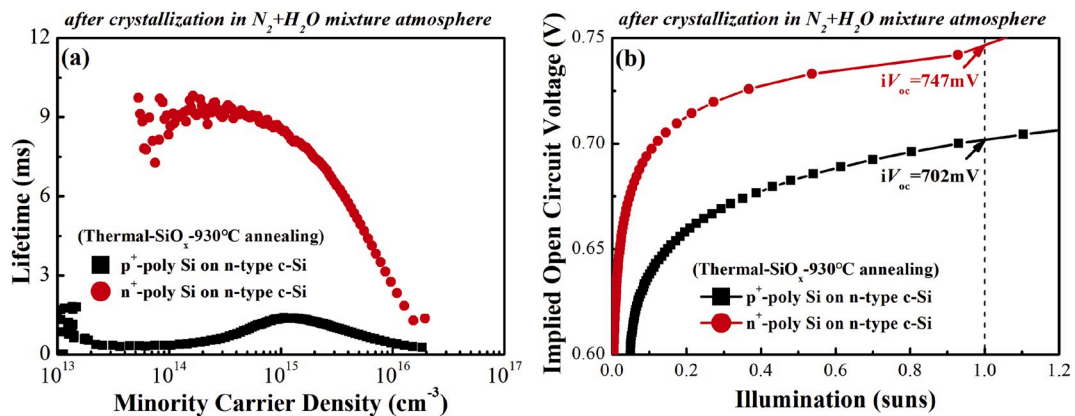

Fig. 2. Comparison of (a) the τ_{eff} spectra and (b) the implied open circuit voltage versus the light intensity of p-TOPCon and n-TOPCon passivated n-c-Si wafers, where the same Thermal-SiO$_x$ was used as the tunnel oxide layer.

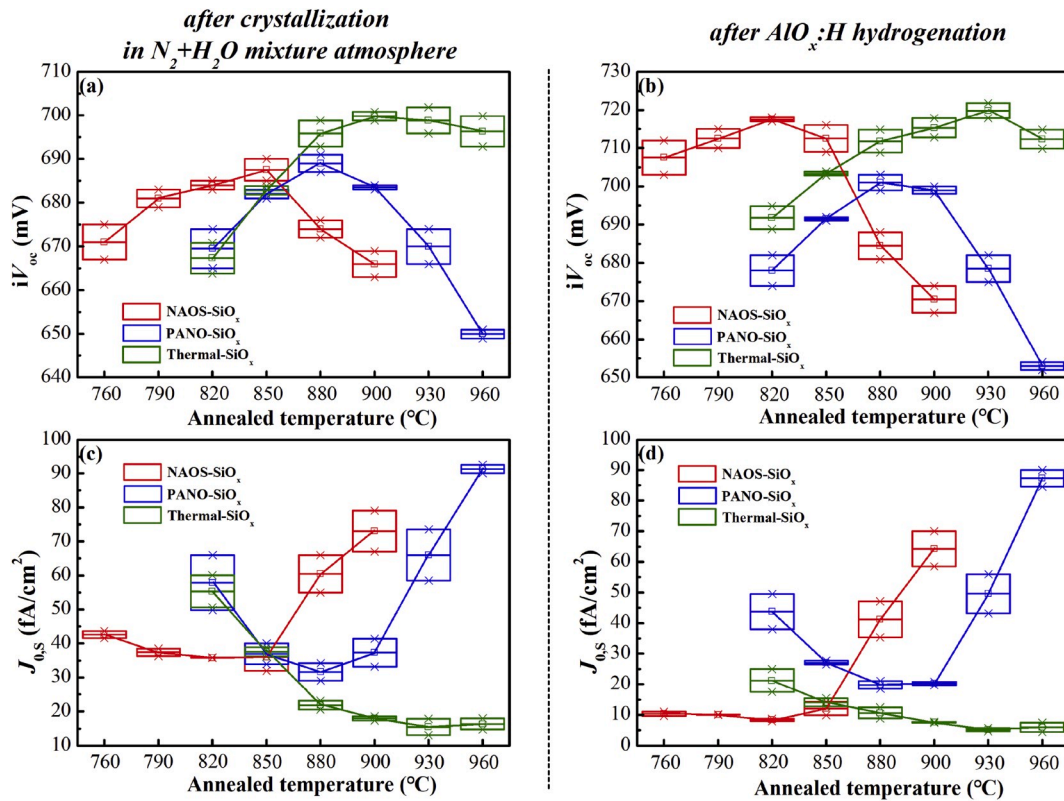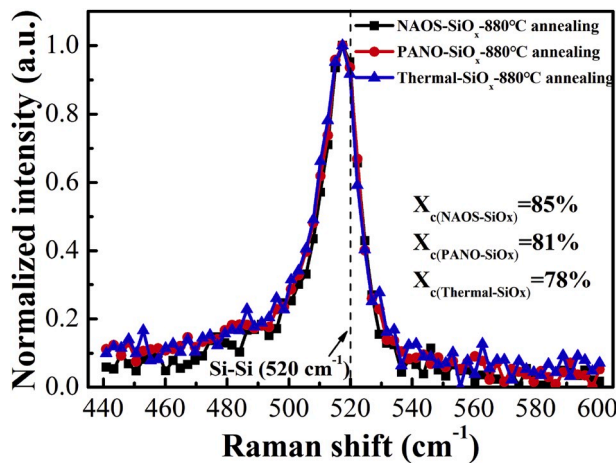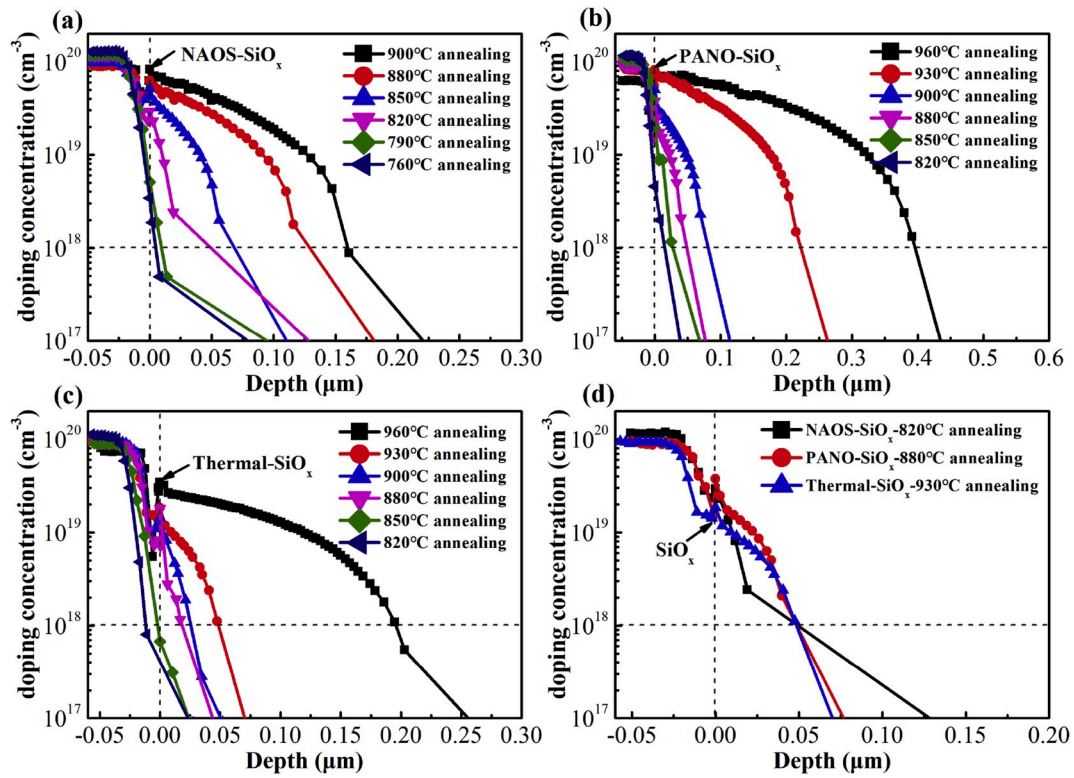**Fig. 3.** The characteristic passivation quality parameters as a function of annealing temperature.

Fig. 4. The normalized data of the Raman spectra taken on the p$^+$-poly-Si with the three kinds of SiO$_x$ annealed at the 880 °C, where X$_C$ is the crystalline ratio calculated by fitting the Raman spectra with three Gaussian components of amorphous phase at 480 cm^{-1}, grain boundary phase at 510 cm^{-1}, and crystalline phase at 520 cm^{-1}.

cm^{-3}. Furthermore, one observation is that the B profiles have a dip at the poly-Si/SiO$_x$ interface. The mechanism of forming such low B density at the interface is not clear at this moment. One speculation is that the dopants in the p$^+$-poly-Si near the SiO$_x$ interface diffuse into the c-Si and leave a low concentration region near the interface, while the SiO$_x$ might have pinholes and microvoids, which leads dopant aggregation in the SiO$_x$ and forms a peak there.
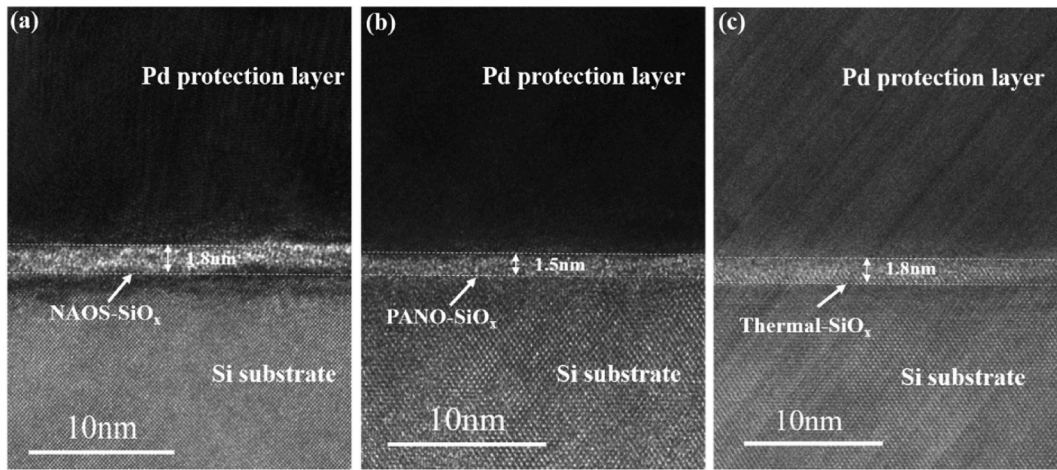
Two factors could affect the B diffusion profiles, which are the SiO$_x$ thickness and its compactness. Logically thinking, the thinner and looser the SiO$_x$ layer, the more pronounced the B diffusion occurs. We did X-

TEM measurements with the results shown in Fig. 6. It appears that the interfaces are not very clear with some non-uniformity. The estimated average thicknesses by multiple measurements at different locations are ~1.8 ± 0.2 nm for the NAOS-SiO$_x$ and the Thermal-SiO$_x$, which is slightly thicker than the PANO-SiO$_x$ (~1.5 ± 0.2 nm). From the thickness estimation, we have the reason to believe that the higher annealing temperature for reaching the optimized passivation with the Thermal-SiO$_x$ could partially result from the slightly thicker SiO$_x$ blocking layer, but the different optimized annealing temperatures between the NAOS-SiO$_x$ and PANO-SiO$_x$ could not be explained by the thickness of the SiO$_x$ layer because the PANO-SiO$_x$ appears thinner than the others. Therefore, other mechanisms need to be explored.

The quality of the chemical bonding configuration is another factor influencing the passivation quality. It has been assumed that the stoichiometric configuration (SiO$_2$) should have the highest compactness and results in the best passivation quality. For figuring out the chemical structures, XPS measurements are normally used to obtain the Si–O bonding configurations of Si^{1+}, Si^{2+}, Si^{3+}, Si^{4+}, corresponding to the number of Si–O bonds on an Si atom [49,50]. As imaged, the SiO$_x$ layer might also change during the high-temperature annealing, such as restructuring the chemical bond configuration and pinhole formation, and thus the ideal XPS measurements should be made with the samples in the p-TOPCon structures after removing the poly-Si layer. However, etching the poly-Si layer in the TOPCon structure is a troublesome process, which could also cause additional damages on the SiO$_x$ layer; therefore we believe that the measurements on the SiO$_x$ layers in the as-grown condition still provides useful information with the closer to the stoichiometric configuration as measured by higher Si^{4+} component, the denser and stable materials and the better passivation forms. Here, we did the XPS measurements on the three SiO$_x$ samples with the results shown in Fig. 7 (a) and Fig. 7 (b), where the Si 2p bond was analyzed to obtain the constituent elements and Si bonding configurations. In order to take into account the charging effects on the measured binding energies, all peaks are calibrated with a C 1s peak of 284.6 eV. A Shirley
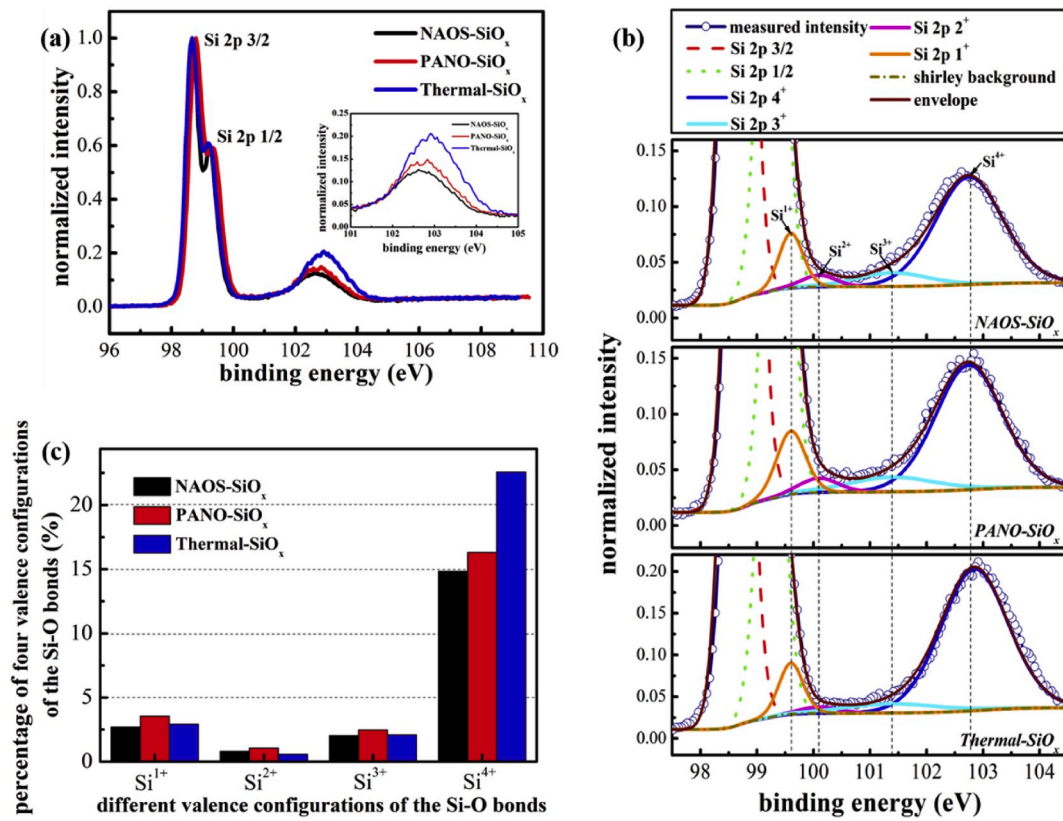
Fig. 5. (a), (b) and (c) are the active B distributions of the samples with the NAOS-SiO$_x$, PANO-SiO$_x$, and Thermal-SiO$_x$, respectively, and (d) compares the samples annealed at the optimized temperatures with the three kinds of SiO$_x$ layers. Note that the horizontal axis is with different scales for different figures for clarity.

Fig. 6. Cross-sectional TEM images of Pd/SiO$_x$/c-Si samples with the three SiO$_x$ films of (a) NAOS-SiO$_x$, (b) PANO-SiO$_x$, and (c) Thermal-SiO$_x$.

background subtraction was applied to the data before fitting the peak components. And we performed a semi-quantitative analysis of the constituents of SiO$_x$ to evaluate the quality of the SiO$_x$ films. The Si substrate peak was fitted as two peaks (Si 2p 3/2 and Si 2p 1/2). And after calibration, Si 2p 3/2 and Si 2p 1/2 of the Si 2p orbital were found at 98.6 eV and 99.2 eV. As observed, no matter which method was used to prepare the SiO$_x$ layer, different valence states have always existed, including Si$_2$O (Si^{1+}), SiO (Si^{2+}), Si$_2$O$_3$ (Si^{3+}), SiO$_2$(Si^{4+}). The higher the content of the component with the high valence state of SiO$_2$ (Si^{4+}), the better the quality of the SiO$_x$ is. In Fig. 7 (b), the Si 2p peak was fitted with four peaks of their positions at 99.6 eV for Si^{1+}, 100.1 eV for Si^{2+}, 101.4 eV for Si^{3+}, and 102.8 eV Si^{4+}. In order to compare the content of different valence states in the three SiO$_x$ samples clearly, we put the silicon contents of the four valence states in one picture, as shown in

Fig. 7 (c). The sample with Thermal-SiO$_x$ exhibits a higher stoichiometric Si^{4+} than the other two samples, which means that the Thermal-SiO$_x$ has better quality and is denser than the others. This result is in agreement with the observation by Moldovan et al. [50]. The slightly thicker and more stoichiometric Thermal-SiO$_x$ layer produces more resistance for B diffusion, and therefore a higher-annealing temperature is needed to reach the optimized B diffusion profile. In addition, the higher Si^{4+} component might result in a lower interface defect states and hence a better passivation quality. The difference in the passivation quality and the optimized annealing temperature between the NAOS--SiO$_x$ and PANO-SiO$_x$ samples are somewhat puzzling. Along the same line of argument, one would expect the PANO-SiO$_x$ should be thicker and more stoichiometric than the NAOS-SiO$_x$, but experimentally no clear such trends are observed as shown in Fig. 7 (a) and 7 (c). One
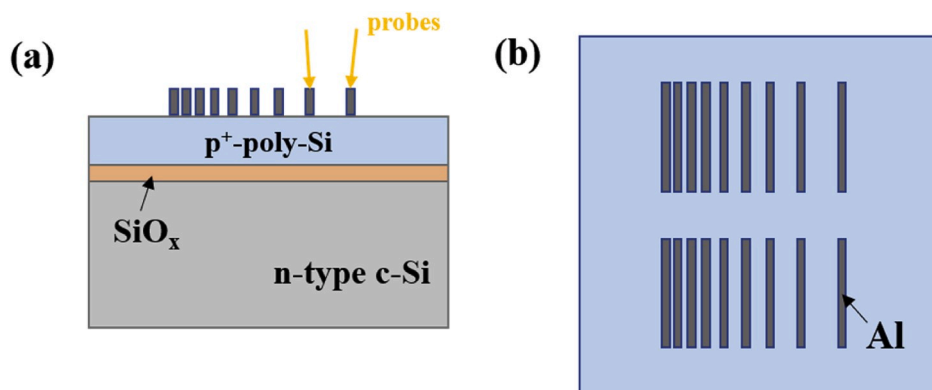
Fig. 7. (a) Comparison of XPS spectra of different SiO_x samples (NAOS-SiO_x, PANO-SiO_x and Thermal-SiO_x) after normalization. The small image as the inset is the energy spectrum comparison of 101eV–105eV after normalization. (b) Fractional fitting (Si 2p 3/2 and Si 2p 1/2, Si^{1+}, Si^{2+}, Si^{3+} and Si^{4+}) of XPS spectra of different SiO_x samples. (c) Comparison of the percentages of four valence configurations of the Si–O bonds in the SiO_x films obtained by fitting the Si 2p XPS spectra of the three kinds of SiO_x samples.
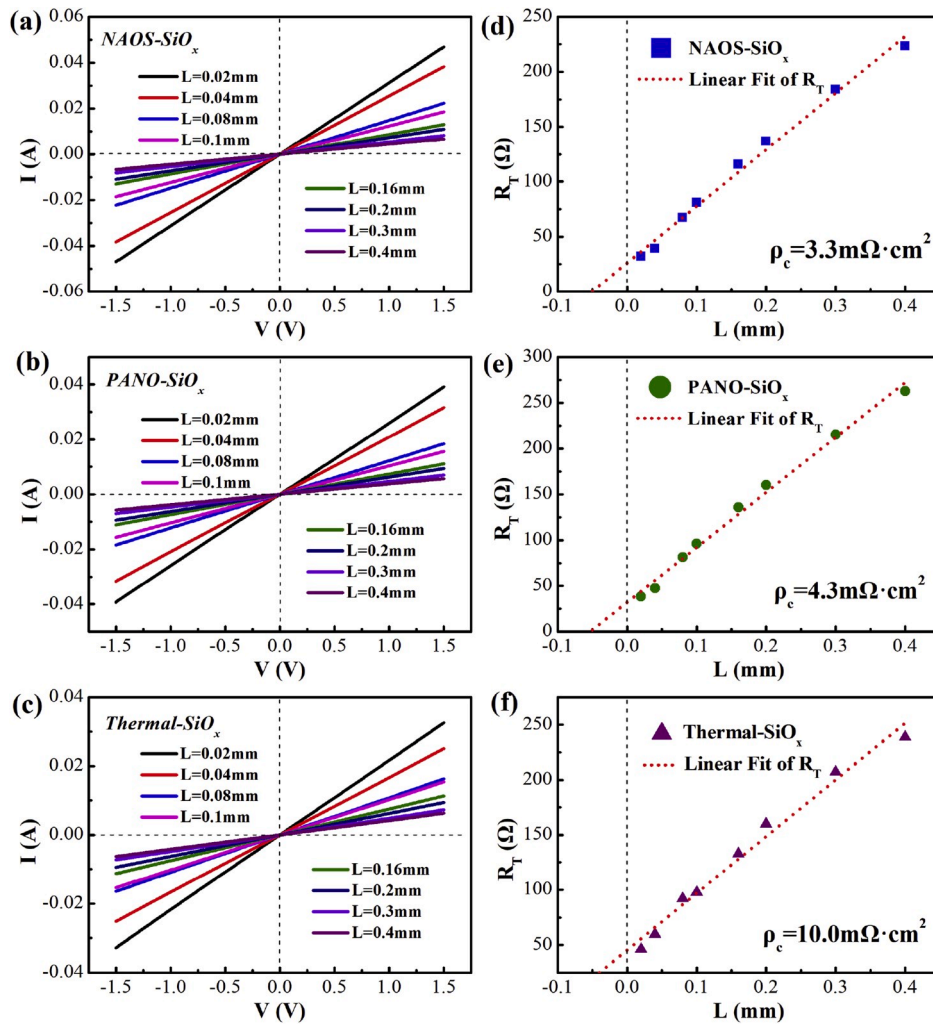
speculation for causing such inconsistency is the incorporation of N in the PANO-SiO_x because it is produced by oxidation with N_2O plasma. Although O has a much stronger electronic negativity than N, some small amount of N could also penetrate into the SiO_x layer. The recent studies by Feldmann et al. [27] showed that the incorporation of N in SiO_x reduces the B diffusion and deteriorates the passivation quality of p-TOPCon structures.

For high-efficiency c-Si solar cells, except for the passivation quality, the electrical performance is another critical parameter influencing the solar cell performance. B-doped p-TOPCon on the n-type c-Si wafer forms a p/n junction, and the I–V curve follows the diode characteristics, and therefore the CS method [36] is not suitable for the contact resistivity (ρ_c) measurements unless a special treatment is used [37,38], while the conductivity of the p^+-poly-Si layer is high enough allowing

the current flows mainly in the p^+-poly-Si layer, and therefore the ρ_c between the metal and the p^+-ploy-Si can be properly measured using the TLM method on the p-TOPCon/SiO_x/n-c-Si structures as shown in Fig. 8. Fig. 9 reveals the ρ_c measurements of the samples with NAOS-SiO_x, PANO-SiO_x, and Thermal-SiO_x and annealed at 820 °C, 880 °C, and 930 °C, respectively, where the left plots show the I–V characteristics and the right plots the total resistance (R_T) of the Al contacts with various gap distances. From Fig. 9, we find that the poly-Si layers on the different SiO_x layers all have the Ohmic characteristics. By comparing the slopes of the I–V curves, as shown in the left plots of Fig. 9, we obtain the ρ_c values from the plot of measured resistances versus the gap distances, as shown in the right plots of Fig. 9. It notes that the ρ_c values of the samples with NAOS-SiO_x, PANO-SiO_x annealed at 820 °C, 880 °C are 3.3 $m\Omega\ cm^2$, 4.3 $m\Omega\ cm^2$, respectively, while the sample with the

Fig. 8. The sketches (a) cross sectional and (b) top views of the samples structure tested using the TLM method.
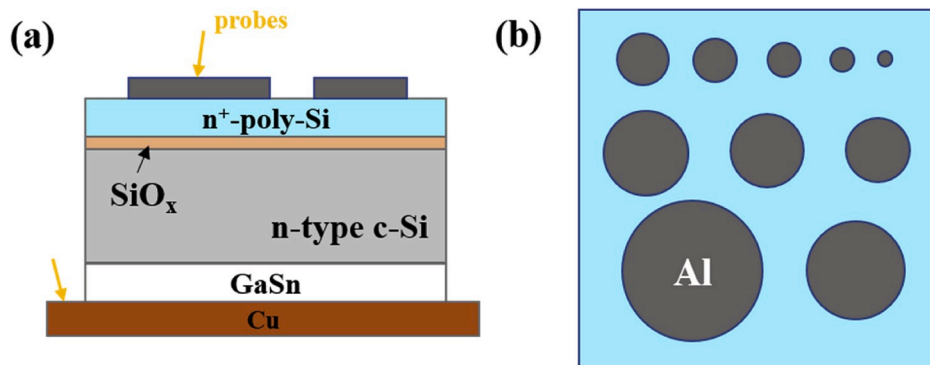
Fig. 9. The TLM ρ_c measurement results of the samples with p$^+$-poly-Si/SiO$_x$/n-c-Si structure, where the SiO$_x$ layers are with the NAOS-SiO$_x$, PANO-SiO$_x$, and Thermal-SiO$_x$ annealed at 820 °C, 880 °C, and 930 °C, respectively, where (a) (b) (c) plot the I–V characteristics and (d) (e) (f) plot the total resistance (R$_T$) of the Al contacts with various gap distances (L). In the right plots, the red dots are the linear fittings. (For interpretation of the references to colour in this figure legend, the reader is referred to the Web version of this article.)
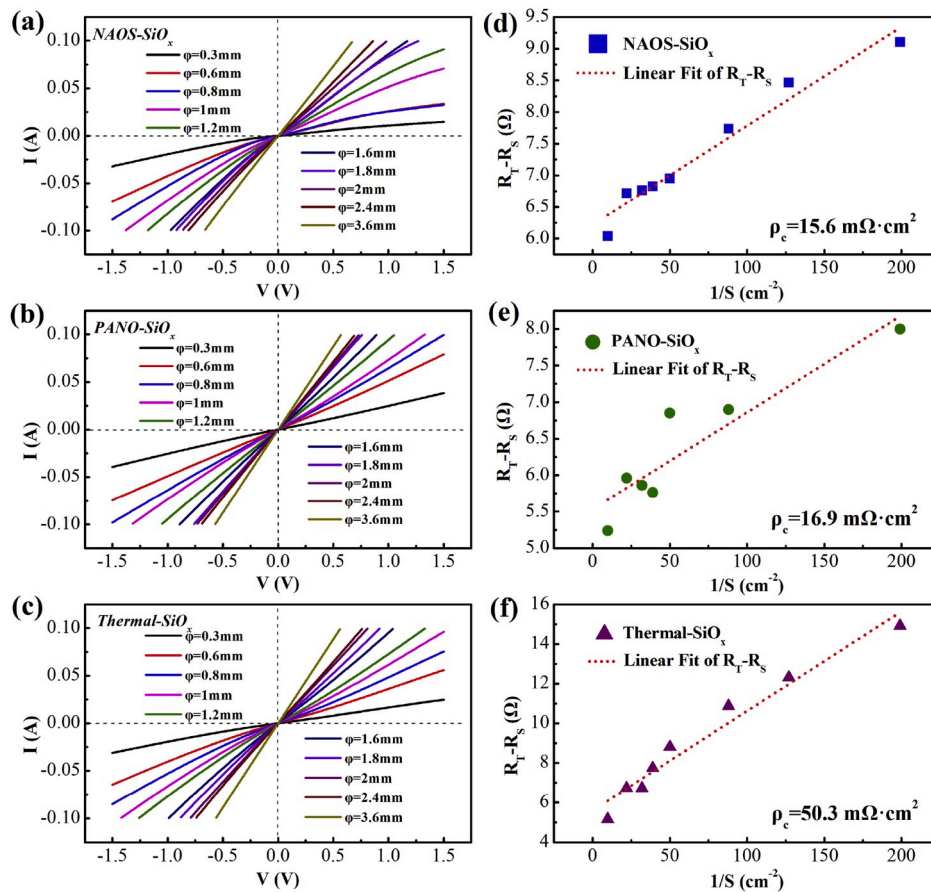
Thermal-SiO$_x$ annealed at 930 °C has the ρ_c of 10.0 mΩ cm^2, which is higher than the other two samples. For this phenomenon, our guess is that the high-temperature annealing may cause the poly-Si layer to be oxidized in some degrees even in the N$_2$ protection because the N$_2$ may not be pure enough to prevent the oxidation completely. The sample with Thermal-SiO$_x$ was annealed at a higher temperature than the other two, and the oxidation was probably more than the others as well.

As motioned above, the TLM does not reveal the resistance information across the SiO$_x$ layer and the p$^+$-ploy-Si on n-c-Si forms a diode preventing the extradition of ρ_c accurately using the CS method. In order

to obtain the reliable ρ_c values, including the SiO$_x$ layer, we made n$^+$-poly-Si on one side of the SiO$_x$ coated n-c-Si wafer for measuring the ρ_c with the CS method on the sample as shown in Fig. 10. Although the results with this sample structure are different from the real p-TOPCon on n-c-Si, the difference in the contact resistivity between the samples reflects the difference contributed by the different SiO$_x$ with the assumption of the same p-poly-Si contact layers and the same n-c-Si substrates. The results are shown in Fig. 11, where most of the I–V curves show linear characteristics, and the ρ_c values are obtained. Once again, the ρ_c value of 50.3 mΩ cm^2 from the sample with Thermal-SiO$_x$ is much

Fig. 10. The sketches of (a) cross sectional and (b) top views of the sample structure tested using the CS method.

Fig. 11. The CS ρ_c measurement results of the samples with n^+-poly-Si/SiO$_x$/n-c-Si structure, where the SiO$_x$ layers are with the NAOS-SiO$_x$, PANO-SiO$_x$, and Thermal-SiO$_x$ annealed at 820 °C, 880 °C, and 930 °C, respectively, where (a) (b) (c) plot the I–V characteristics and (d) (e) (f) plot the difference between the total resistance (R_T) and the spreading resistance (R_S) of the reciprocal of Al electrode area with different diameters. In the right plots, the red dots are the linear fittings. (For interpretation of the references to colour in this figure legend, the reader is referred to the Web version of this article.)

higher than the values of ~16 mΩ cm^2 from the other two samples. In addition, the overall ρ_c values are higher than reported in the literature [2,51], but they are still low enough for high-efficiency solar cells as proven by simulation study [51,52]. The reason for the high ρ_c value could result from the thicker and denser SiO$_x$ layer.

4. Summary

We have systematically studied the B-doped p^+-poly-Si/SiO$_x$ passivated contact on n-type c-Si wafers, where the SiO$_x$ layer was made with three methods of hot nitric acid oxidation, plasma-assisted nitrous-oxide (N$_2$O) gas oxidation, and thermal oxidation. The experiment results show that the passivation quality significantly depends on the SiO$_x$ properties. The thermally oxidized SiO$_x$ shows the best passivation quality of iV_{oc} = 722 mV, τ_{eff} = 1.56 ms at 1×10^{15} cm^{-3}, and $J_{0,S}$ = 5.95 fA/cm^2, which is one of the highest passivation parameters reported in the literature. The nitric acid and N$_2$O plasma oxidized SiO$_x$ layers show poorer passivation quality than the thermally oxidized ones. In addition, the optimized annealing temperatures for achieving the best passivation quality are different for the samples with different SiO$_x$ layers, where the chemically oxidized SiO$_x$ needs 820 °C, the N$_2$O plasma oxidized SiOx 880 °C, and thermally oxidized SiO$_x$ 930 °C. We made various structural and compositional analyses and found that the B diffusion is one important parameter determining the passivation quality. The samples with the corresponding best passivation quality have the same B diffusion profile which decays towards the inside of the wafer and reaches 1×10^{18} cm^{-3} at about 50 nm from the SiO$_x$/c-Si interface. The XPS results show that the thermally oxidized SiO$_x$ has the highest Si^{4+} component, which indicates the more SiO$_2$ component in the film. The contact resistivity measurements show that the thermally oxidized SiO$_x$ has a higher contact resistivity than the other two samples,

but the absolute value is still low enough for achieving high-efficiency TOPCon solar cells.

CRediT authorship contribution statement

Xueqi Guo: Conceptualization, Data curation, Formal analysis. **Mingdun Liao:** Conceptualization, Data curation, Formal analysis. **Zhe Rui:** Data curation, Formal analysis. **Qing Yang:** Data curation, Formal analysis. **Zhixue Wang:** Data curation, Formal analysis. **Chunhui Shou:** Funding acquisition, Investigation, Methodology. **Waner Ding:** Investigation, Methodology. **Xijia Luo:** Data curation, Formal analysis. **Yuhong Cao:** Investigation, Methodology. **Jiaping Xu:** Investigation, Methodology. **Liming Fu:** Project administration, Resources. **Yuheng Zeng:** Project administration, Supervision, Validation. **Baojie Yan:** Supervision, Validation, Visualization, Writing - original draft, Writing - review & editing. **Jichun Ye:** Funding acquisition, Project administration, Writing - original draft.

Appendix A. Supplementary data

Supplementary data to this article can be found online at https://doi.org/10.1016/j.solmat.2020.110487.

References

[1] F. Feldmann, M. Bivour, C. Reichel, M. Hermle, S.W. Glunz, Passivated rear contacts for high-efficiency n-type Si solar cells providing high interface passivation quality and excellent transport characteristics, Sol. Energy Mater. Sol. Cells 120 (2014) 270–274.

[2] A. Richter, J. Benick, F. Feldmann, A. Fell, M. Hermle, S.W. Glunz, n-Type Si solar cells with passivating electron contact: identifying sources for efficiency limitations by wafer thickness and resistivity variation, Sol. Energy Mater. Sol. Cells 173 (2017) 96–105.

[3] M. Rienäcker, A. Merkle, U. Römer, H. Kohlenberg, J. Krügener, R. Brendel, R. Peibst, Recombination behavior of photolithography-free back junction back contact solar cells with carrier-selective polysilicon on oxide junctions for both polarities, Energy Procedia 92 (2016) 412–418.

[4] M.K. Stodolny, J. Anker, B.L.J. Geerligs, G.J.M. Janssen, B.W.H.v.d. Loo, J. Melskens, R. Santbergen, O. Isabella, J. Schmitz, M. Lenes, J.-M. Luchies, W.M. M. Kessels, I. Romijn, Material properties of LPCVD processed n-type polysilicon passivating contacts and its application in PERPoly industrial bifacial solar cells, Energy Procedia 124 (2017) 635–642.

[5] S. Duttagupta, N. Nandakumar, P. Padhamnath, J.K. Buatis, R. Stangl, A.G. Aberle, monoPoly™ cells: large-area crystalline silicon solar cells with fire-through screen printed contact to doped polysilicon surfaces, Sol. Energy Mater. Sol. Cells 187 (2018) 76–81.

[6] Y. Chen, D. Chen, C. Liu, Z. Wang, Y. Zou, Y. He, Y. Wang, L. Yuan, J. Gong, W. Lin, X. Zhang, Y. Yang, H. Shen, Z. Feng, P.P. Altermatt, P.J. Verlinden, Mass production of industrial tunnel oxide passivated contacts (i-TOPCon) silicon solar cells with average efficiency over 23% and modules over 345 W, Prog. Photovoltaics Res. Appl. 27 (2019) 827–834.

[7] E. Yablonovitch, T. Gmitter, R.M. Swanson, Y.H. Kward, A 720 mV open circuit voltage SiOₓ:c-Si:SiOₓ double heterostructure solar cell, Appl. Phys. Lett. 47 (1985) 1211–1213.

[8] J.Y. Gan, R.M. Swanson, Polysilicon emitters for silicon concentrator solar cells, Proc. IEEE Conf Photovolt Spec. (1990) 245–250.

[9] R. Peibst, U. Römer, Y. Larionova, M. Rienäcker, A. Merkle, N. Folchert, S. Reiter, M. Turcu, B. Min, J. Krügener, D. Tetzlaff, E. Bugiel, T. Wietler, R. Brendel, Working principle of carrier selective poly-Si/c-Si junctions: is tunnelling the whole story? Sol. Energy Mater. Sol. Cells 158 (2016) 60–67.

[10] Z. Zhang, Y. Zeng, C.-S. Jiang, Y. Huang, M. Liao, H. Tong, M. Al-Jassim, P. Gao, C. Shou, X. Zhou, B. Yan, J. Ye, Carrier transport through the ultrathin silicon-oxide layer in tunnel oxide passivated contact (TOPCon) c-Si solar cells, Sol. Energy Mater. Sol. Cells 187 (2018) 113–122.

[11] F. Feldmann, M. Bivour, C. Reichel, H. Steinkemper, M. Hermle, S.W. Glunz, Tunnel oxide passivated contacts as an alternative to partial rear contacts, Sol. Energy Mater. Sol. Cells 131 (2014) 46–50.

[12] F. Feldmann, M. Simon, M. Bivour, C. Reichel, M. Hermle, S.W. Glunz, Efficient carrier-selective p- and n-contacts for Si solar cells, Sol. Energy Mater. Sol. Cells 131 (2014) 100–104.

[13] S. Mack, F. Feldmann, A. Moldovan, M. Lenes, J.M. Luchies, A. Wolf, Impact of surface morphology and interfacial oxide thickness on passivation quality of p⁺ polysilicon passivating contacts, in: 35ᵗʰ European Photovoltaic Solar Energy Conference and Exhibition, 2018, pp. 587–590.

[14] S. Mack, M. Lenes, J.M. Luchies, A. Wolf, P-Type silicon solar cells with passivating rear contact formed by LPCVD p⁺ polysilicon and screen printed Ag metallization, Phys. Status Solidi RRL 13 (2019) 201900064.

[15] G. Nogay, J. Stuckelberger, P. Wyss, E. Rucavado, C. Allebé, T. Koida, M. Morales-Masis, M. Despeisse, F.-J. Haug, P. Löper, C. Ballif, Interplay of annealing temperature and doping in hole selective rear contacts based on silicon-rich silicon-carbide thin films, Sol. Energy Mater. Sol. Cells 173 (2017) 18–24.

[16] A. Ingenito, G. Nogay, Q. Jeangros, E. Rucavado, C. Allebé, S. Eswara, N. Valle, T. Wirtz, J. Horzel, T. Koida, M. Morales-Masis, M. Despeisse, F.-J. Haug, P. Löper, C. Ballif, A passivating contact for silicon solar cells formed during a single firing thermal annealing, Nat. Energy 3 (2018) 800–808.

[17] M.K. Stodolny, J. Anker, C.J.J. Tool, M. Koppes, A.A. Mewe, P. Manshanden, M. Lenes, I.G. Romijn, Novel schemes of p⁺ polySi hydrogenation implemented in industrial 6'' bifacial front-and-rear passivating contacts solar cells, in: 35ᵗʰ European Photovoltaic Solar Energy Conference and Exhibition, 2018, pp. 414–417.

[18] D. Yan, A. Cuevas, S.P. Phang, Y. Wan, D. Macdonald, 23% efficient p-type crystalline silicon solar cells with hole-selective passivating contacts based on physical vapor deposition of doped silicon films, Appl. Phys. Lett. 113 (2018), 061603.

[19] A. Morisset, R. Cabal, B. Grange, C. Marchat, J. Alvarez, M.E. Gueunier-Farret, S. Dubois, J.P. Kleider, Conductivity and surface passivation properties of boron-doped poly-silicon passivated contacts for c-Si solar cells, Phys. Status Solidi 216 (2018) 1800603.

[20] Z. Xin, Z.P. Ling, P. Wang, J. Ge, C. Ke, K.B. Choi, A.G. Aberle, R. Stangl, Ultra-thin atomic layer deposited aluminium oxide tunnel layer passivated hole-selective contacts for silicon solar cells, Sol. Energy Mater. Sol. Cells 191 (2019) 164–174.

[21] B. Nemeth, D.L. Young, M.R. Page, V. LaSalvia, S. Johnston, R. Reedy, P. Stradins, Polycrystalline silicon passivated tunneling contacts for high efficiency silicon solar cells, J. Mater. Res. 31 (2016) 671–681.

[22] M. Schnabel, B.W.H.v.d. Loo, W. Nemeth, B. Macco, P. Stradins, W.M.M. Kessels, D.L. Young, Hydrogenation passivation of poly-Si/SiOₓ contacts for Si solar cells using Al₂O₃ studied with deuterium, Appl. Phys. Lett. 112 (2018) 203901.

[23] A.S. Kale, W. Nemeth, S.P. Harvey, M. Page, D.L. Young, S. Agarwal, P. Stradins, Effect of silicon oxide thickness on polysilicon based passivated contacts for high-efficiency crystalline silicon solar cells, Sol. Energy Mater. Sol. Cells 185 (2018) 270–276.

[24] D.L. Young, B.G. Lee, D. Fogel, W. Nemeth, V. LaSalvia, S. Theingi, M. Page, M. Young, C. Perkins, P. Stradins, Gallium-doped poly-Si:Ga/SiO₂ passivated emitters to n-Cz wafers with iVₒc > 730 mV, IEEE J. Photovolt. 7 (2017) 1640–1645.

[25] R.V.D. Vossen, F. Feldmann, A. Moldovan, M. Hermle, Comparative study of differently grown tunnel oxide for p-type passivating contacts, Energy Procedia 124 (2017) 448–454.

[26] A. Richter, J. Benick, R. Müller, F. Feldmann, C. Reichel, M. Hermle, S.W. Glunz, Tunnel oxide passivating electron contacts as full-area rear emitter of high-efficiency p-type silicon solar cells, Prog. Photovoltaics Res. Appl. 26 (2018) 579–586.

[27] F. Feldmann, J. Schön, J. Niess, W. Lerch, M. Hermle, Studying dopant diffusion from Poly-Si passivating contacts, Sol. Energy Mater. Sol. Cells 200 (2019) 109978.

[28] U. Romer, R. Peibst, T. Ohrdes, B. Lim, J. Krugener, T. Wietler, R. Brendel, Ion implantation for poly-Si passivated back-junction back-contacted solar cells, IEEE J. Photovolt. 5 (2015) 507–514.

[29] R. Peibst, Y. Larionova, S. Reiter, M. Turcu, R. Brendel, D. Tetzlaff, J. Krugener, T. Wietler, U. Hohne, J.-D. Kahler, H. Mehlich, S. Frigge, Implement of N⁺ and P⁺ POLO junction on front and rear side of double-side contact industral silicon solar cells, in: Proc. Of 32ⁿᵈ European Photovoltaic Conference and Exhibition, 2016, pp. 323–327.

[30] M. Winter, S. Bordihn, R. Peibst, R. Brendel, J. Schmidt, Degradation and regeneration of n⁺-doped poly-Si surface passivation on p-type and n-type Cz-Si under illumination and dark annealing, IEEE J. Photovolt. 10 (2020) 423–430.

[31] W. Shockley, W.T.J. Read, Statistics of recombination of holes and electrons, Phys. Rev. 87 (1952) 835–842.

[32] R.N. Hall, Electron-hole recombination in germanium, Phys. Rev. 87 (1952) 387.

[33] Z. Zhang, M. Liao, Y. Huang, X. Guo, Q. Yang, Z. Wang, T. Gao, C. Shou, Y. Zeng, B. Yan, J. Ye, Improvement of surface passivation of tunnel oxide passivated contact structure by thermal annealing in mixture of water vapor and nitrogen environment, Solar RRL 3 (2019) 1900105.

[34] Y. Huang, Y. Zeng, Z. Zhang, X. Guo, M. Liao, C. Shou, S. Huang, B. Yan, J. Ye, UV-Raman scattering of thin film Si with ultrathin silicon oxide tunnel contact for high efficiency crystal silicon solar cells, Sol. Energy Mater. Sol. Cells 192 (2019) 154–160.

[35] S.S. Cohen, Contact resistance and methods for its determination, Thin Solid Films 104 (1983) 361–379.

[36] R.H. Cox, H. Strack, Ohmic contacts for GaAs devices, Solid State Electron. 10 (1967) 1213–1218.

[37] S. Theingi, W. Nemeth, D.L. Young, P. Stradins, B.G. Lee, Measuring diode resistivity of passivated Contacts, in: 44ᵗʰ IEEE Photovoltaic Specialist Conference, PVSC), Washington, DC, USA, 2017, pp. 1832–1834.

[38] W. Wang, H. Lin, Z. Yang, Z. Wang, J. Wang, L. Zhang, M. Liao, Y. Zeng, P. Gao, B. Yan, J. Ye, An expanded Cox and Strack method for precise extraction of specific contact resistance of transition metal oxide/n-silicon heterojunction, IEEE J. Photovolt. 9 (2019) 1113–1120.

[39] H.K. Asuha, O. Maida, M. Takahashi, H. Iwasa, Nitric acid oxidation of Si to form ultrathin silicon dioxide layers with a low leakage current density, J. Appl. Phys. 94 (2003) 7328–7335.

[40] Y. Huang, M. Liao, Z. Wang, X. Guo, C. Jiang, Q. Yang, Z. Yuan, D. Huang, J. Yang, X. Zhang, Q. Wang, H. Jin, M. Al-Jassim, C. Shou, Y. Zeng, B. Yan, J. Ye, Ultrathin silicon oxide prepared by in-line plasma-assisted N₂O oxidation (PANO) and the application for n-type polysilicon passivated contact, Sol. Energy Mater. Sol. Cells 208 (2020) 110389.

[41] H. Tong, M. Liao, Z. Zhang, Y. Wan, D. Wang, C. Quan, L. Cai, P. Gao, W. Guo, H. Lin, C. Shou, Y. Zeng, B. Yan, J. Ye, A strong-oxidizing mixed acid derived high-quality silicon oxide tunneling layer for polysilicon passivated contact silicon solar cell, Sol. Energy Mater. Sol. Cells 188 (2018) 149–155.

[42] T. Gao, Q. Yang, X. Guo, Y. Huang, Z. Zhang, Z. Wang, M. Liao, C. Shou, Y. Zeng, B. Yan, G. Hou, X. Zhang, Y. Zhao, J. Ye, An industrially viable TOPCon structure with both ultra-thin SiOₓ and n⁺-poly-Si processed by PECVD for p-type c-Si solar cells, Sol. Energy Mater. Sol. Cells 200 (2019) 109926.

[43] K. Bothe, R. Sinton, J. Schmidt, Fundamental boron-oxygen-related carrier lifetime limit in mono- and multicrystalline silicon, Prog. Photovoltaics Res. Appl. 13 (2005) 287–296.

[44] J. Schmidt, K. Bothe, Structure and transformation of the metastable boron- and oxygen-related defect center in crystalline silicon, Phys. Rev. B 69 (2004), 024107.

[45] Z. Rui, Y. Zeng, X. Guo, Q. Yang, Z. Wang, C. Shou, W. Ding, J. Yang, X. Zhang, Q. Wang, H. Jin, M. Liao, S. Huang, B. Yan, J. Ye, On the passivation mechanism of poly-silicon and thin silicon oxide on crystal silicon wafers, Sol. Energy 194 (2019) 18–26.

[46] Z. Wang, Z. Liu, M. Liao, D. Huang, X. Guo, Z. Rui, Q. Yang, W. Guo, J. Sheng, C. Shou, B. Yan, Z. Yuan, Y. Zeng, J. Ye, Effective gettering of in-situ phosphorus-doped polysilicon passivating contact prepared using plasma-enhanced chemical-vapor deposition technique, Sol. Energy Mater. Sol. Cells 206 (2020) 110256.

[47] R.A. Street, Hydrogenated Amorphous Silicon, Cambridge University Press, Cambridge, 1991.

[48] M. Stutzmann, R.A. Street, Donor states in hydrogenated amorphous silicon and germanium, Phys. Rev. Lett. 54 (1985) 1836–1839.

[49] A. Moldovan, F. Feldmann, G. Krugel, M. Zimmer, J. Rentsch, M. Hermle, A. Roth-Fölsch, K. Kaufmann, C. Hagendorf, Simple cleaning and conditioning of silicon surfaces with UV/ozone Sources☆, Energy Procedia 55 (2014) 834–844.

[50] A. Moldovan, F. Feldmann, M. Zimmer, J. Rentsch, J. Benick, M. Hermle, Tunnel oxide passivated carrier-selective contacts based on ultra-thin SiO_2 layers, Sol. Energy Mater. Sol. Cells 142 (2015) 123–127.

[51] A. Richer, J. Benick, R. Muller, F. Feldmann, C. Reichel, M. Hermle, S.W. Glunz, Tunnel oxide passivating electron contacts as full-area rear emitter of high-efficiency p-type silicon solar cells, Prog. Photovoltaics Res. Appl. 26 (2017) 579–586.

[52] Y. Zeng, Q. Yang, Y. Wan, Z. Yang, M. Liao, Y. Huang, Z. Zhang, X. Guo, Z. Wang, P. Gao, C.-H. Wu, B. Yan, J. Ye, Numerical exploration for high-efficiency structure design and free-energy loss analysis of polysilicon passivated contact p-type silicon solar cell, Sol. Energy 178 (2019) 249–256.